Ritter, O., Junge, A., Dawes, G. J. K. (1998): New equipment and processing for magnetotelluric remote reference observations. - Geophysical Journal International, 132, 3, pp. 535—548.

DOI: https://doi.org/10.1046/j.1365-246X.1998.00440.x

Geophys. J. Int. (1998) **132,** 535–548

New equipment and processing for magnetotelluric remote reference observations

Oliver Ritter,[1] Andreas Junge[2] and Graham J. K. Dawes[3]

[1] *GeoForschungsZentrum Potsdam, Telegrafenberg,* D-14473 *Potsdam, Germany. E-mail: oritter@gfz.potsdam.de*
[2] *Institut für Meteorologie und Geophysik, Universität Frankfurt, Feldbergstrasse* 47, D-60323 *Frankfurt, Germany*
[3] *Department of Geology and Geophysics, University of Edinburgh, Grant Institute, West Mains Road, Edinburgh* EH9 3JW, *UK*

Accepted 1997 August 29. Received 1997 August 28; in original form 1997 January 24

SUMMARY

Robust estimates of magnetotelluric and geomagnetic response functions are determined using the coherency and expected uniformity of the magnetic source field as quality criteria. The method is applied on data sets of three simultaneously recording sites. For the data acquisition we used a new generation of geophysical equipment (S.P.A.M. MkIII), which comprises novel concepts of parallel computing and networked, digital data transmission. The data-processing results show that the amount of noise on the horizontal components of the magnetic field varies considerably in time, between sites and over the frequency range. The removal of such contaminated data beforehand is essential for most data-processing schemes, as the magnetic channels are usually assumed to be free of noise. The standard remote reference method is aimed at reducing bias in response function estimates. However, this does not necessarily improve their precision as our results clearly show. With our method, on the other hand, we can filter out source field irregularities, thereby providing suitable working conditions for the robust algorithm, and eventually obtain considerably improved results. Contrary to previous concepts, we suggest rejecting as much data as feasible in order to concentrate on the remaining parts of high-quality observations.

Key words: data processing, electromagnetic instrumentation, magnetotellurics.

1 INTRODUCTION

The magnetotelluric (MT) method is applied to determine the electrical conductivity distribution beneath the Earth's surface. Electric currents in the atmosphere give rise to magnetic field variations which induce electric currents in the Earth. For MT measurements, orthogonal components of the electric and magnetic fields are recorded as time variations at the surface of the Earth. In the frequency-domain representation, the electric and horizontal magnetic field components are linearly related by the impedance tensor $\boldsymbol{Z}$, a so-called response function of the Earth. The aim of electromagnetic data-processing procedures is to estimate these response functions as accurately as possible.

It is often rather difficult to acquire high-quality MT data because the measurements rely on a highly variable strength of the natural electromagnetic excitation. The signal amplitudes of the vertical variation field, for instance, are of the order of 10 000 times smaller than the static main field. More severe problems are caused by civilization, which produces all kinds of electromagnetic signals, for example from mains power supplies, electric railways, electric fences, radar and radio transmitters, etc. (Szarka 1988). These sources generate very coherent large-amplitude electromagnetic signals which are superimposed on the natural variation field. Such artificially produced events are therefore not electromagnetic noise, although they are considered noise by magnetotelluric practitioners. In practice, it is very difficult to distinguish coherent cultural signals from the natural electromagnetic fields in which we are interested. We aim to separate signal from noise at the data-processing stage by analysing data from frequently repeated experiments (long recording times) using modern statistical methods. However, to tackle the problems we require not only sophisticated data-processing procedures but also highly specialized geophysical instrumentation. Good equipment is particularly important, as it is usually impossible to recover erroneous field recordings by data-analysis methods.

There has been an enormous progress in MT data-processing algorithms over the past two decades; a review is given by Junge (1996). Progress has mainly come about through two developments—robust statistics and the remote reference method. Robust algorithms are based on data-adaptive weighting schemes, which aim to detect and reject outliers from a majority of *well-behaved* samples (e.g. Egbert & Booker 1986; Chave, Thomson & Ander 1987). The remote reference method requires simultaneously recorded horizontal

GJI000 18/2/98 09:07:37 3B2 version 5.20
The Charlesworth Group, Huddersfield 01484 517077

magnetic fields from two sites which ideally have only components of correlated signal and uncorrelated noise (Goubau, Gamble & Clarke 1978; Gamble, Goubau & Clarke 1979). The most promising results are achieved by a combination of both methods—a robust remote reference processing (e.g. Larsen 1989; Jones *et al.* 1989).

However, a robust remote reference processing is still a bivariate data-analysis tool, as a consequence of which the measured electromagnetic signals must be divided into noise-free dependent and noisy independent channels. This division is introduced for theoretical reasons, while we know of course that in practice all channels are affected by noise. Data-processing methods which allow noise in all channels have been introduced by Park & Chave (1984) and Chave & Thomson (1989), and more recently by Larsen *et al.* (1996) and Egbert (1997). It is extremely difficult, though, to estimate reliably the covariance matrix of the noise, which is necessary for a multivariate approach. A multivariate data processing will be superior to all other methods if the nature of the noise can be recognized correctly. However, its numerical application is rather costly and it might sometimes lead to incorrect results (Larsen 1989; Egbert 1997).

A new method is thus proposed in this paper. This method uses physical properties of the magnetic source field—its homogeneity and spatial coherence—to simplify the processing problem. Its application is demonstrated on noisy field data from southern Scotland, in which some apparently useless response function results are converted into interpretable curves. For the fieldwork, we used a new generation of geophysical instruments (S.P.A.M. MkIII), which facilitate simultaneous recordings of electromagnetic field data from many stations at high frequencies.

2 RESPONSE FUNCTION ESTIMATION

In the frequency domain, the complex relation between the electromagnetic signals can be written

$$\begin{pmatrix} E_x \\ E_y \end{pmatrix} = \begin{pmatrix} Z_{xx} & Z_{xy} \\ Z_{yx} & Z_{yy} \end{pmatrix} \begin{pmatrix} B_x \\ B_y \end{pmatrix}, \tag{1}$$

where $\mathbf{E}$ is the electric field in mV km^{-1}, $\mathbf{B}$ is the magnetic field in nT and Z_{ij} are the components of $\boldsymbol{Z}$. We assume plane-wave sources, dependence on frequency and Cartesian coordinate systems. x, y and z are defined to be positive when pointing towards the north, the east and downwards, respectively. A non-zero vertical magnetic field component is generated if lateral conductivity variations are of the order of the induction range of the observations. The geomagnetic response functions $\mathscr{A}$, $\mathscr{B}$ are defined in a similar manner to eq. (1):

$$B_z = \mathscr{A} B_x + \mathscr{B} B_y . \tag{2}$$

In practice, the response functions are estimated from imperfect data. From different samples we aim to choose our parameters so that the misfit to the data is minimized by some norm, e.g. L_1 or L_2. Generally, we must solve linear equations of the type

$$Z = aX + bY + \delta Z . \tag{3}$$

Z is the output channel of the linear system, which is normally associated with E_x, E_y or B_z, while X and Y are the input channels, associated with the horizontal magnetic fields B_x and B_y. The noise term δZ is assumed to affect only the output channel Z. Then, the solution for the response function a (and similarly for b) using the least-squares (LS) method is

$$a = \frac{\langle ZX^* \rangle \langle YY^* \rangle - \langle ZY^* \rangle \langle YX^* \rangle}{\langle XX^* \rangle \langle YY^* \rangle - \langle XY^* \rangle \langle YX^* \rangle} . \tag{4}$$

The bracketed terms indicate cross- or auto-spectra, calculated and stacked from individual time segments and averaged over a certain frequency band; the asterisk denotes a complex conjugate.

2.1 The remote reference method

Consider now all channels to be combinations of signal and noise, indicated by the indices S and N, e.g. $X := X_S + X_N$, etc. By definition, statistical noise is uncorrelated with the signal. If, additionally, noise between different channels is assumed to be uncorrelated and the signal is correlated, only the first term on the right-hand side of eq. (5) is non-zero:

$$\langle XY^* \rangle = \langle X_S Y_S^* \rangle + \langle X_S Y_N^* \rangle + \langle X_N Y_S^* \rangle + \langle X_N Y_N^* \rangle . \tag{5}$$

Auto-spectra, on the other hand, will always be contaminated:

$$\langle XX^* \rangle = \langle X_S X_S^* \rangle + \underbrace{\langle X_N X_N^* \rangle}_{=\text{bias}} , \tag{6}$$

and eventually cause biased response function estimates. Being based on the idea that magnetic fields recorded at two different sites have only uncorrelated noise components, the classical remote reference technique reduces the effects of bias (Goubau *et al.* 1978; Gamble *et al.* 1979). Using the input components from two sites, the impedance tensor can be rewritten as

$$\boldsymbol{Z}_r = (\mathbf{E}\mathbf{B}_r^*)(\mathbf{B}\mathbf{B}_r^*)^{-1} ; \qquad \mathbf{E}\mathbf{B}^* := \begin{pmatrix} \langle E_x B_x^* \rangle & \langle E_x B_y^* \rangle \\ \langle E_y B_x^* \rangle & \langle E_y B_y^* \rangle \end{pmatrix}, \tag{7}$$

where the subscript r denotes the fields of a remote site. Now, only cross-spectra of horizontal magnetic field components of local and remote sites appear in the solution of $\boldsymbol{Z}_r$. The estimation of $\boldsymbol{Z}_r$ is unbiased if the noise between the two sites is uncorrelated.

2.2 The source-field criterion

For magnetotelluric measurements in mid-latitudes in the period range below 10 000 s, the wavelengths of the inducing electromagnetic fields are generally large compared to their penetration depth in the Earth. Then, the influence of the source geometry on the response functions can be neglected; the source field is called *quasi-uniform*. For any two sites under these constraints, the horizontal magnetic field variations are connected by magnetic response functions (MRF) which are time-independent:

$$\mathbf{T} = (\mathbf{B}\mathbf{B}_r^*)(\mathbf{B}_r\mathbf{B}_r^*)^{-1} ; \qquad \mathbf{T} := \begin{pmatrix} T_{xx} & T_{xy} \\ T_{yx} & T_{yy} \end{pmatrix} . \tag{8}$$

For exactly uniform source fields and for a horizontally layered earth, $\mathbf{T} = \mathbf{I}$ for all frequencies. Lateral conductivity anomalies, however, also give rise to anomalous horizontal magnetic fields which are superimposed on the source fields. For the general case, the MRFs are therefore frequency-dependent, complex valued and different from unity (Larsen

GJI000 18/2/98 09:08:33 3B2 version 5.20
The Charlesworth Group, Huddersfield 01484 517077

et al. 1996). The gradient of the anomalous component is largest close to the edges of a lateral conductivity contrast, but decreases rapidly with increasing distance from the boundary (Banks, Irving & Livelybrooks 1993; Weaver 1994). Thus, the observed MRFs of densely spaced sites should, in general, be close to unity.

The ratio of predicted to measured signal energy between output and input channels is given by the multiple quadratic coherencies r_x^2 and r_y^2, where r_x refers to B_x and r_y to B_y as output channels:

$$r_x^2 = \frac{T_{xx}\langle B_x B_{xr}^* \rangle + T_{xy}\langle B_x B_{yr}^* \rangle}{\langle B_{xr} B_{xr}^* \rangle} . \tag{9}$$

The results for the multiple coherency can be biased due to noise in the auto-spectra in the denominator and in the response functions. The coherency will be close to 1, however, if local and remote sites are only little affected by noise. Processing results for single site and remote reference are the same if $r_{x,y}^2 = 1$.

The proposed source-field criterion causes data rejection based on two aspects: (1) if horizontal magnetic field components between two sites have low coherencies (coherency criterion) and (2) if the response functions are considerably different from unity (target criterion). The method is applied iteratively by comparison of both horizontal magnetic fields of the local site with all or some combinations of the reference site(s). Events with inconsistent horizontal magnetic field data are thereby removed step by step, leaving a reduced but cleaned data set for the final robust stacking. A more detailed discussion of the method is given in Section 4.

The appropriateness of the target criterion depends on the data set as the frequency range of the observations, the geological complexity and the distance between the sites have to be considered. From our experience, however, the target criterion can be used in general.

2.3 The iterative robust algorithm

Generally, the true noise distribution in our observations is unknown; however, applying least-square methods the noise has to be normally distributed to obtain maximum-likelihood estimates. Robust methods aim to single out moderate number of data that are not normally distributed. In that respect, response functions estimated with robust methods are less sensitive to a moderate amount of *bad* data or to an inadequately chosen statistical model. Robust processing of AMT data by automatic weighting algorithms has been widely used, for example by dividing the time-series into segments of equal length, estimating auto- and cross-spectra from each segment and stacking the weighted spectra after applying a smoothing window in the frequency domain.

As weighting of data can cause downward-biased estimation of variance, a better estimate is obtained using Huber's (1981) expression for asymptotic variances (*cf*. Egbert & Booker 1986, Appendix). However, the estimation of the number of degrees of freedom v depends on the number of stacked spectra and the smoothing window for which the equivalent bandwidth may be used to estimate v under the assumption that adjacent raw spectral values are statistically independent. As this assumption seems to be often violated, an attempt is made to estimate the true value of v.

With the assumption that the weighted residuals are normally distributed with variance σ^2, the variance of the single-time-segment residuals obeys approximately a χ_v^2 distribution with v degrees of freedom. An estimate of v is obtained directly from the distribution of σ. A property of the χ_v^2 distribution is that its expectation is $E\{\sigma^2\} = v\sigma^2$ and its variance is $\mathrm{var}\{\sigma^2\} = 2v(\sigma^2)^2$. It follows that

$$\hat{v} = \frac{2(E\{\sigma^2\})}{\mathrm{var}\{\sigma^2\}} . \tag{10}$$

However, application of eq. (10) shows that the hypothetical estimate of v from the shape of the spectral window is often severely overestimated.

In this context we describe a method developed by Junge (1990, 1992, 1994) which has been tested extensively on a huge volume of data from various regions. The algorithm has proven to be fast, reliable and efficient. The method combines two parts: (1) the χ^2 criterion and (2) the consistency criterion. (1) The χ^2 criterion examines whether a single-event spectrum fits into the global view of the majority of all data. Accordingly, the influence of a single-event spectrum is increased or decreased by a robust weighting scheme. (2) The consistency criterion reduces non-stationary contributions in the response functions by iteratively replacing a certain amount of the *bad* data with predicted values. A more detailed description of the algorithm is given in Appendix A.

In the present form, the estimation of confidence limits for the response functions is still based on a parametric model for the distribution of the noise. Chave *et al.* (1987) and Larsen *et al.* (1996) have suggested using the non-parametric jackknife method instead, as it will generally be more robust against deviations from the expected model.

3 S.P.A.M. MKIII

Before we concentrate further on aspects of the data processing, we would like to introduce the newly developed S.P.A.M. MkIII instrument which was used to collect our remote-referenced audiomagnetotelluric data sets.

S.P.A.M. systems are short-period automatic magnetotelluric instruments developed since 1980 by Graham Dawes at the University of Edinburgh; work on the new generation of instruments started in 1990 (Dawes 1990). Today, S.P.A.M. MkIII systems are successfully used by a number of research institutions across Europe, including the geophysical equipment pools of NERC and GeoForschungsZentrum Potsdam and the geophysics departments of the universities in Edinburgh, Frankfurt and TU Berlin. An early summary of the ideas behind the instrument can be found in Ritter & Dawes (1992); more up-to-date summaries are given by Ritter (1995) and Nascimento (1997).

S.P.A.M. MkIII operates as a networked instrument. This network consists of geophysical sensors with distributed analogue and digital processing and control units. Networks can be very simple, for example a standard five-component MT configuration, or they can be complex systems, where many compatible S.P.A.M. MkIII modules (for example from different research institutions) are interconnected.

The network communication is based on bi-directional digital data transfer, and all devices on the network are synchronized. The timing of S.P.A.M. MkIII can also be

GJI000 18/2/98 09:09:05 3B2 version 5.20
The Charlesworth Group, Huddersfield 01484 517077

controlled by GPS clocks in order to synchronize recordings of separated networks over large distances. Because digitally transmitted signals do not deteriorate with distance, reference fields from remote sites can be collected together with signals from local sites. Furthermore, the instrument is not restricted to recording electromagnetic data only, but can be used more generally for geophysical data acquisition, for example a combination of seismic and electromagnetic recordings. Improved computational power allows parts of the analogue signal conditioning to be replaced by digital signal processing. Consequently, the design of the analogue sections has become simpler, which means improved reliability and better noise figures. The computational heart of S.P.A.M. MkIII is the *transputer*, a microprocessor with built-in parallel processing and network support. Parallel execution of processes enables a digital and concurrent generation of the frequency bands used for the data processing. This is an important improvement over existing instruments as it results in shorter recording times. Until now, different frequency bands had to be recorded sequentially.

All parts of the instrument are built in a highly modular fashion to allow test facilities, modifications, replacements or enhancements of parts of the system without having to change everything. The overall power consumption is greatly improved over older generations of S.P.A.M. (and comparable instruments) because new low-power devices can be used throughout the system.

A S.P.A.M. MkIII network consists of four major nodes (see Fig. 1).

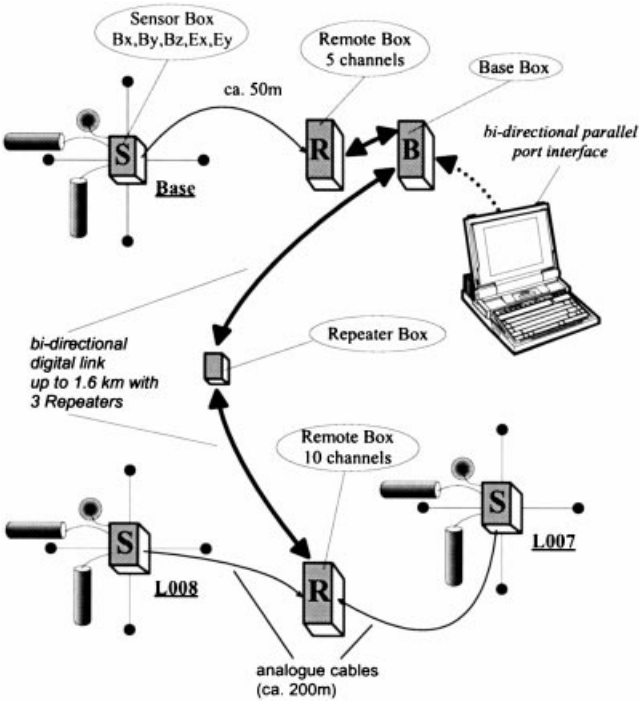

Figure 1. S.P.A.M. MkIII is a networked geophysical instrument. Analogue signals from geophysical sensors are preconditioned at the sensor nodes S and then transferred to the remote node(s) R. In remote boxes, analogue and digital signal processing is performed and the data are forwarded to the base node B in digital form, as time-series and/or frequency spectra. The base node controls the entire network and analyses all incoming data streams. Repeater nodes are necessary to drive long cables.

(1) The *sensor node*: this is used to connect various geophysical sensors (for example induction coil magnetometers, electrodes, seismometers, etc.). All necessary signal preconditioning and power supplies are included. The sensor node provides one channel board of the correct type for each sensor.

(2) The *remote node*: analogue signals from the sensor node(s) in the frequency range 2kHz–DC are captured, further bandpass filtered, optionally notch filtered, and amplified using automatic, software-controlled gain ranging. All parts of the analogue signal path can be monitored in real-time. Eventually, analogue signals are converted to digital data and subsequently digital data processing is performed.

Fig. 2 shows a diagram of S.P.A.M. MkIII's binary decimation and processing scheme to generate (narrow) frequency bands for the data analysis. The raw time-series data are low-pass filtered and decimated in octave steps. Low-pass-filtered time-series data can subsequently be high-pass filtered, to create bandpass-filtered data streams. Low- and high-pass corner frequency settings are variable in octave steps ('power of two'). Adjacent or overlapping time segments can be chosen for the FFT. All data can be forwarded to the base node—via high-speed serial data transmission—as the original time-series, as decimated and low-pass-filtered time-series, as bandpass-filtered time-series or as calibrated frequency spectra. Any mixture is possible and all time-series are continuous streams of data which can be stored and/or further processed at the base node.

(3) The *base-node*: this receives GPS signals and controls the entire network. Only one base node per network is permitted. All control registers (switches, gains, filters, multiplexers, overload detectors, etc.) in all attached remote and sensor nodes are set and/or read from the base node. The base node collects all time- and/or frequency-domain data sent over the network from the remote nodes and performs real-time data processing. The time-series data and the stacked results can be stored on an internal hard disk and/or be transferred to a laptop personal computer (PC).

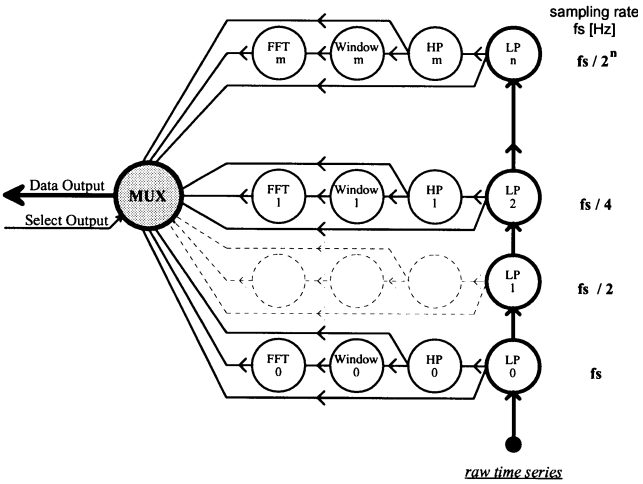

Figure 2. S.P.A.M. MkIII's digital data filtering and decimation scheme. Low-pass and high-pass corner frequency settings are variable in octave steps. All data can be transmitted as original time-series, as decimated and low-pass-filtered time-series, as bandpass filtered time-series or as calibrated frequency spectra. Any mixture is possible and all time-series are continuous streams of data. (MUX is a software multiplexer.)

GJI000 18/2/98 09:09:33 3B2 version 5.20
The Charlesworth Group, Huddersfield 01484 517077

The PC serves as the front-end for user interaction and as a graphics terminal during normal operation. However, it can be disconnected (and re-connected later) if S.P.A.M. MkIII is configured to run unattended, for example to collect and process data in an overnight run. The PC is also used to boot the whole transputer network, as all necessary data and program files can be sent from the PC to all transputers in the network.

(4) The *repeater node*: this is used to refresh digital signals if they are attenuated or otherwise weakened by the communication media (e.g. long copper cables).

4 EXAMPLES USING FIELD DATA

The field data were recorded at a location in southeastern Scotland in the vicinity of the Southern Upland Fault complex, approximately 35 km southeast of Edinburgh. In total, we measured electromagnetic data at seven sites with five-component MT configurations. Using the new facilities of S.P.A.M. MkIII, three sites were always recorded simultaneously. During the survey, the location of the BASE site remained fixed while the other sites were recorded in pairs, at varying distances from the reference point. To discuss the application of the methods described in this paper we concentrate on the spread of sites with the widest extensions: sites BASE, L007 and L008. The distance between site BASE and the travelling sites is 1600 m; the distance between L007 and L008 is 350 m (see Fig. 1). For clarity, we focus on the processing results of the geomagnetic response functions, although the algorithms work equally well for the estimation of the impedance tensor.

For the data processing, the continuously recorded time-series are divided into adjacent segments of fixed lengths (see Table 1). All data segments are cosine tapered and Fourier transformed. The frequency-domain data are corrected for the influence of the instrument response functions, and the calibrated Fourier coefficients are divided into sub-bands, with centre frequencies equally distributed on a logarithmic scale. For each band and all channels, smoothed auto- and cross-spectra estimates are computed. Final response functions are calculated by stacking the single-event spectra from all frequency bands with the iterative robust algorithm from Section 2.3.

Table 1. The data are recorded in six adjacent and one overlapping frequency band; the second and third columns give the actual low-pass and high-pass settings of the digital bandpass filters. For the highest frequency band, the length of a time segment was set to 512 samples; for all other frequency bands a length of 256 samples was chosen. The fifth column lists the overall amount of events for a given segment length. The sampling rate is four times the low-pass corner frequency. The overlapping band 6 is activated to improve the resolution for the longest-period recordings at approximately 100 s.

	low pass	high pass	samples	total events
Band 0	128 Hz	16 Hz	512	1267
Band 1	16 Hz	4 Hz	256	2902
Band 2	4 Hz	1 Hz	256	2441
Band 3	1 s	4 s	256	509
Band 4	4 s	16 s	256	151
Band 5	16 s	128 s	256	35
Band 6	32 s	128 s	256	16

Fig. 3 shows the results of an automatic, robust, single site processing of all available data sets. The geomagnetic response functions for site L008 show a substantial vertical magnetic field anomaly varying smoothly and consistently over most parts of the frequency range. The type of curve is also in good agreement with results from other sites in the area and fits nicely onto a set of long-period data (not shown). The results of sites L007 and BASE, however, look very different from L008,

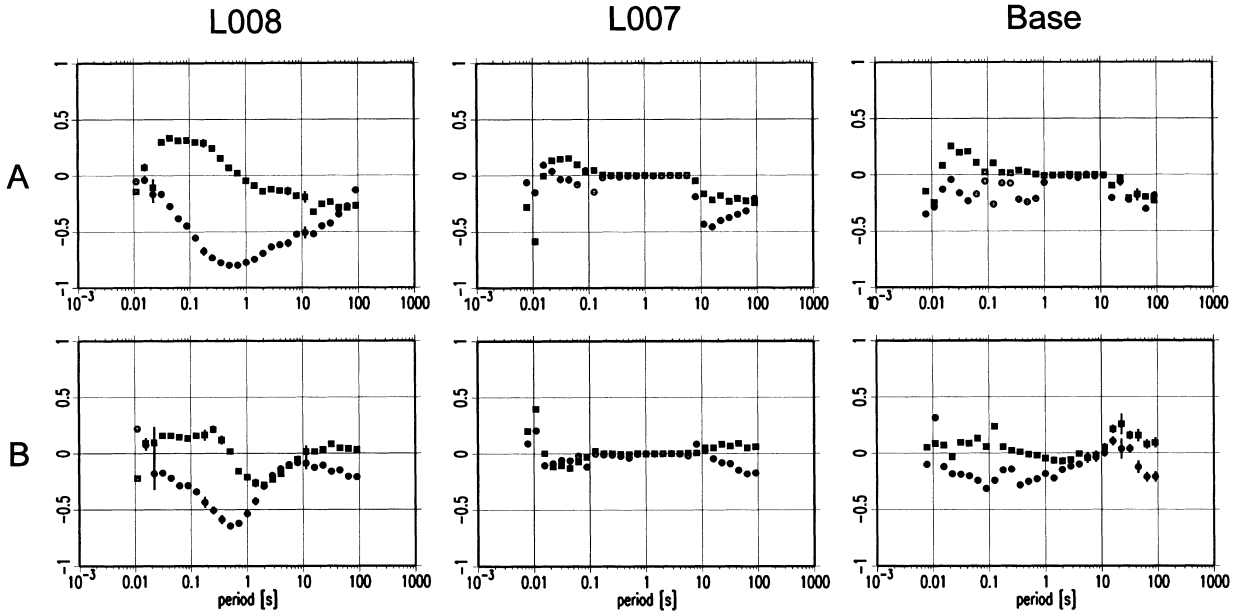

Figure 3. Robust single-site processing of sites L008, L007 and BASE (from left to right) using all available data. The $\mathscr{A}$ and $\mathscr{B}$ response functions [in real (circles) and imaginary (squares) parts] are plotted in the upper and lower sections of the graphs. Clearly, the results for sites L007 and BASE are severely damaged by noise.

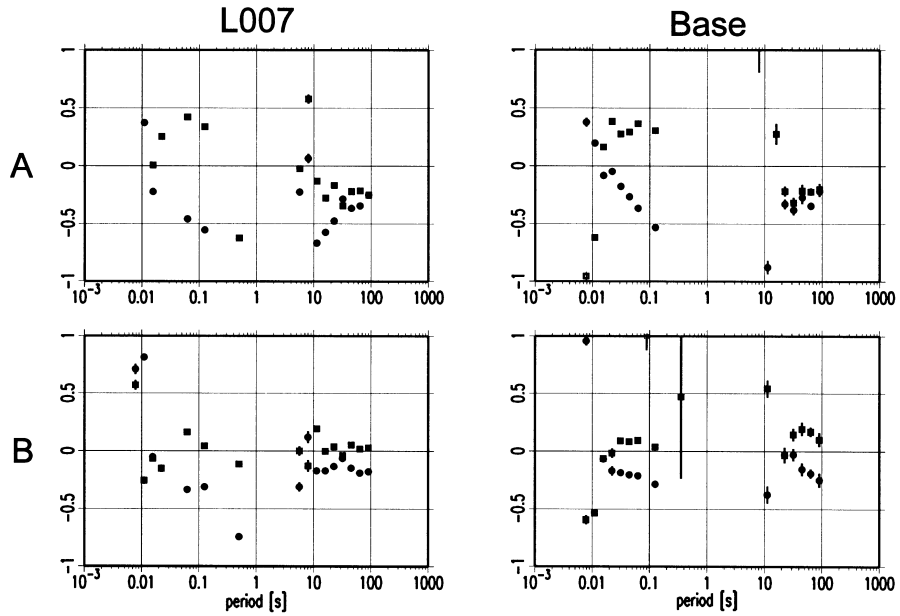

Figure 4. Robust remote reference processing of sites L007 and BASE using all available data. L008 serves as the reference site. The effects of noise are so strong that the remote reference method becomes unstable.

although one would expect similar response functions, considering the relatively small extensions of the station array. The data of these two sites are obviously severely disturbed, the curves look non-physical, and furthermore, the coherencies between vertical and horizontal magnetic components are very low. The error bars are small, but only because the number of estimates is large (see Table 1).

Fig. 4 shows no improvement if we simply apply the remote reference method to sites L007 and BASE using L008 as the reference site. The method depends on both local and remote fields and it appears that noise on the local fields is so strong that the response function estimates become unstable. If we simply replace the horizontal magnetic fields of the local sites with those from the remote site, we obtain the results shown in Fig. 5. Clearly, these *pseudo*-remote reference curves are considerably improved over those of Fig. 4. Now, most of the expected structures can be recognized. Obviously, the outcome is still prone to bias, possibly due to lateral conductivity changes and because the response function estimates rely on auto-spectra. In any case, the pseudo-remote reference results indicate that the problem is connected with poor horizontal magnetic fields at both local sites. For the remote reference

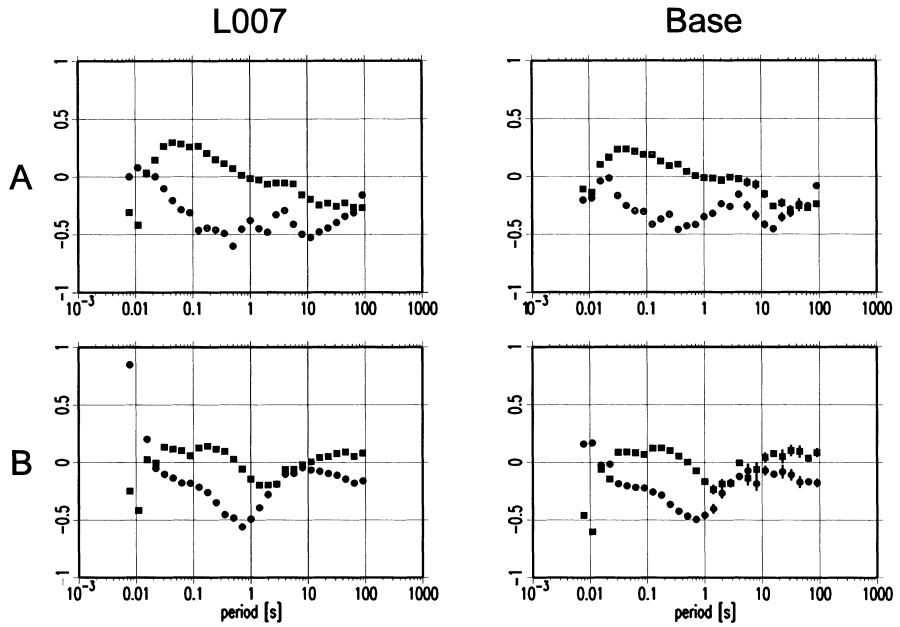

Figure 5. Robust pseudo-remote reference processing of sites L007 and Base using all available data. The local horizontal magnetic fields are replaced by those from site L008. The response function results for the local sites are improved compared to those from Figs 3 and 4. This means that (1) the horizontal fields are strongly disturbed at both local sites and (2) the remote reference method is extremely sensitive to noise in the local fields.

GJI000 18/2/98 09:09:49 3B2 version 5.20
The Charlesworth Group, Huddersfield 01484 517077

method to function properly we must ensure that noise at local and remote sites is uncorrelated, and—just as important—that the signal is spatially coherent. While it is extremely difficult to detect and separate coherent noise, it is straightforward to examine the coherency of the source field between the sites.

The robust algorithm can generally be applied to solve linear, bivariate problems, for example to obtain robust estimates of the MRFs of eq. (8). The MRF curves between L008 and the local sites L007 and BASE are shown in Figs 6(a) and (b), respectively. We observe mostly a close-to-unity response for T_{xx} and T_{yy}, as is expected for densely spaced sites. However, the effects of noise are also visible, for example in the period range 0.1–10 s in $\mathscr{R}eT_{xx}$(L007) and between 0.01 and 0.1 s in $\mathscr{R}eT_{xx}$(BASE). In particular, the abrupt transition from 0.5 to 1 of $\mathscr{R}eT_{xx}$(L007) at 10 s cannot be explained by a geological feature. It is most likely that the whole effect of continuously decreasing values in the period range 0.1–10 s is caused by some strong local noise source in combination with little natural signal energy. Also conspicuous are the deviations from zero in the imaginary parts at the highest frequencies at L007. We cannot distinguish between phase shifts caused by anomalous fields and those from near-field source effects if they are coherent, but the period range coincides with the strongly scattered part of the otherwise very smooth response function curves of L008 in Fig. 3. For the remaining parts, however, T_{xx} and T_{yy} in Figs 6(a) and (b) are—within reasonable bounds—close to unity. T_{xy} and T_{yx}, which are not shown, are zero within their error bars.

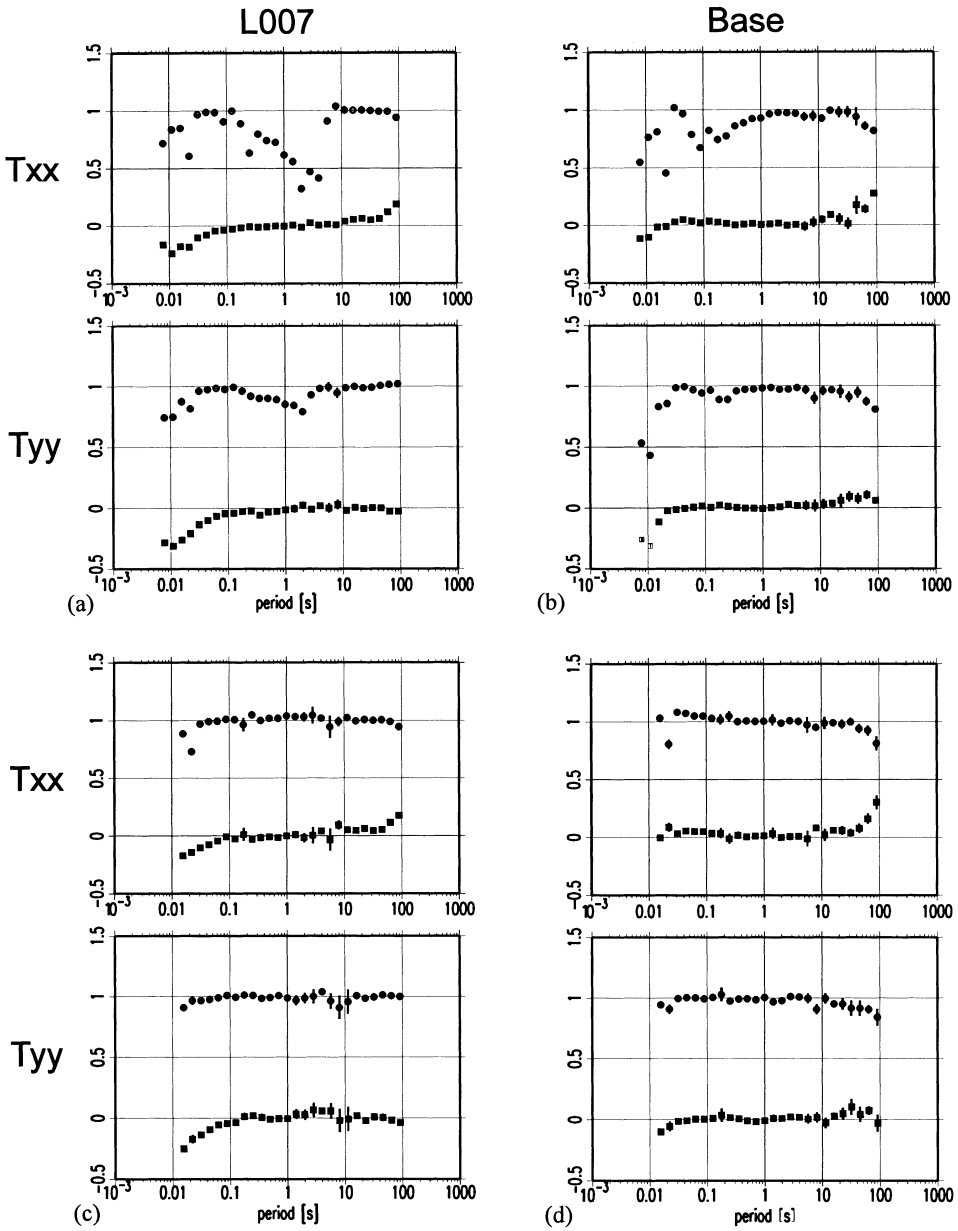

Figure 6. Robust estimation of the MRFs between local sites L007 and BASE using L008 as the reference: (a) and (b) using all available data; (c) and (d) using the reduced data set after application of the source-field criterion. The MRFs in (a) and (b) show at some periods deviations from the expected close-to-unity response and have poor statistical properties. With the reduced data set in (c) and (d), we observe the expected close-to-unity response over the whole frequency range. The deviation of the imaginary parts at the highest frequencies is preserved by the target criterion.

Hence, the source field criterion from Section 2.2 is applied for a reprocessing of the data. The coherency threshold is set to 0.8 and the MRFs are allowed to vary within a radius of 0.2 around unity in the complex plane. Both limits have been determined empirically. They depend on the amount and quality of the data and are adjusted accordingly. The data set contains six synchronously recorded horizontal magnetic field components of three sites, which leaves various possible channel combinations. In the example, the source field criterion is applied step by step to the following eight channel combinations:

$$B_x(\mathrm{L008}) = T_{xx}B_x(\mathrm{BASE}) + T_{xy}B_y(\mathrm{BASE}),$$

$$B_x(\mathrm{L008}) = T_{xx}B_x(\mathrm{L007}) + T_{xy}B_y(\mathrm{L007}),$$

$$B_y(\mathrm{L008}) = T_{yx}B_x(\mathrm{BASE}) + T_{yy}B_y(\mathrm{BASE}),$$

$$B_y(\mathrm{L008}) = T_{yx}B_x(\mathrm{L007}) + T_{yy}B_y(\mathrm{L007}),$$

$$B_x(\mathrm{L008}) = T_{xx}B_x(\mathrm{BASE}) + T_{xy}B_y(\mathrm{L007}),$$

$$B_x(\mathrm{L008}) = T_{xx}B_x(\mathrm{L007}) + T_{xy}B_y(\mathrm{BASE}),$$

$$B_y(\mathrm{L008}) = T_{yx}B_x(\mathrm{BASE}) + T_{yy}B_y(\mathrm{L007}),$$

$$B_y(\mathrm{L008}) = T_{yx}B_x(\mathrm{L007}) + T_{yy}B_y(\mathrm{BASE}).$$

Putting the assumed noise-free component on the left side of the equation amplifies the bias of the response functions. Thus, the noisy segments of the time-series automatically yield deviations from unity and, consequently, will be removed from the data set. The effects on the data selection process are demonstrated in Figs 7 and 8. Fig. 7(a) examines coherencies and MRFs between B_x(L008) and $B_{x,y}$(BASE) at a frequency of 16 Hz. The top diagram shows the multiple coherency, plotted for each event; the solid line indicates the threshold of 0.8. The estimates are derived from 1267 time-series segments (events) of 512 samples each (see Table 1). All those events with coherencies below 0.8 are rejected; 203 out of 1267 in the example. Plotted in the diagram just below the coherencies are the magnitudes of the single-event MRFs. Note that the events are ordered in time. The two smaller diagrams at the bottom left, on the other hand, concentrate on the stationarity of the MRFs. The MRFs are plotted in the complex plane and the circles indicate the areas of acceptance: 470 events of a total of 1064 with coherencies better than 0.8 fail to lie within a distance of 0.2 of the target response functions (1, 0) and (0, 0). Overall, 673 events are rejected and 594 are promoted to the next step which compares B_x(L008) with $B_{x,y}$(L007). At this stage, which is not shown, 397 events are accepted. Fig. 7(b) shows the third step, in which B_y(L008) is examined with respect to $B_{x,y}$(BASE). Now the data appear cleaned, because only 33 events out of 397 are rejected. Most of the coherencies are very close to 1 and most of the data are within the target, that is they are arranged as expected within close bounds to a unity response. After all eight decimation steps, 308 events are accepted.

The situation changes completely in Fig. 8, where the data are examined at 45 Hz, close to the frequency of mains power supplies (50 Hz) which generate near-field signals with much higher amplitudes than the natural signals. The main part of that signal is already filtered by S.P.A.M. MkIII but there is always leakage to the neighbouring frequencies. Thus, more than 1000 events out of 1267 fail to reach the required coherency of 0.8 at the first hurdle. The data section between events 350 and 600, in which more events fulfil the coherency criterion, could indicate an interval of increased natural signal activity. The distribution of the MRFs in the complex plane appears almost as random, and after the third decimation step in Fig. 8(b), only eight out of 1267 events are acceptable. These eight events are eventually reduced to four after all eight iteration steps.

Comparison of the total number of events in Table 1 with the amount of accepted events in Table 2 shows how significantly

Table 2. The total number of recorded events in comparison with the number of accepted events after application of the source-field criterion. The amount of rejected data varies considerably between the observation frequencies. Note the high number of accepted data for frequencies which are multiples of the Schumann resonance.

	evaluation frequency or period/accepted events						
Band 0	128 Hz	90 Hz	64 Hz	45 Hz	32 Hz	22 Hz	16 Hz
total: 1267	2	3	98	4	513	79	308
Band 1	16 Hz	11 Hz	8 Hz	5.6 Hz	4 Hz		
total: 2902	493	91	432	24	7		
Band 2	4 Hz	2.8 Hz	2 Hz	1.4 Hz	1 Hz		
total: 2441	38	58	111	136	131		
Band 3	1 s	1.4 s	2 s	2.8 s	4 s		
total: 509	24	23	37	18	25		
Band 4	4 s	5.6 s	8 s	11.3 s	16 s		
total: 151	10	8	8	7	36		
Band 5	16 s	22.7 s	32 s	45.5 s	64 s		
total: 35	7	17	14	10	13		
Band 6	32 s	45.5 s	64 s	90 s			
total: 16	5	5	6	5			

GJI000 18/2/98 09:09:58 3B2 version 5.20
The Charlesworth Group, Huddersfield 01484 517077

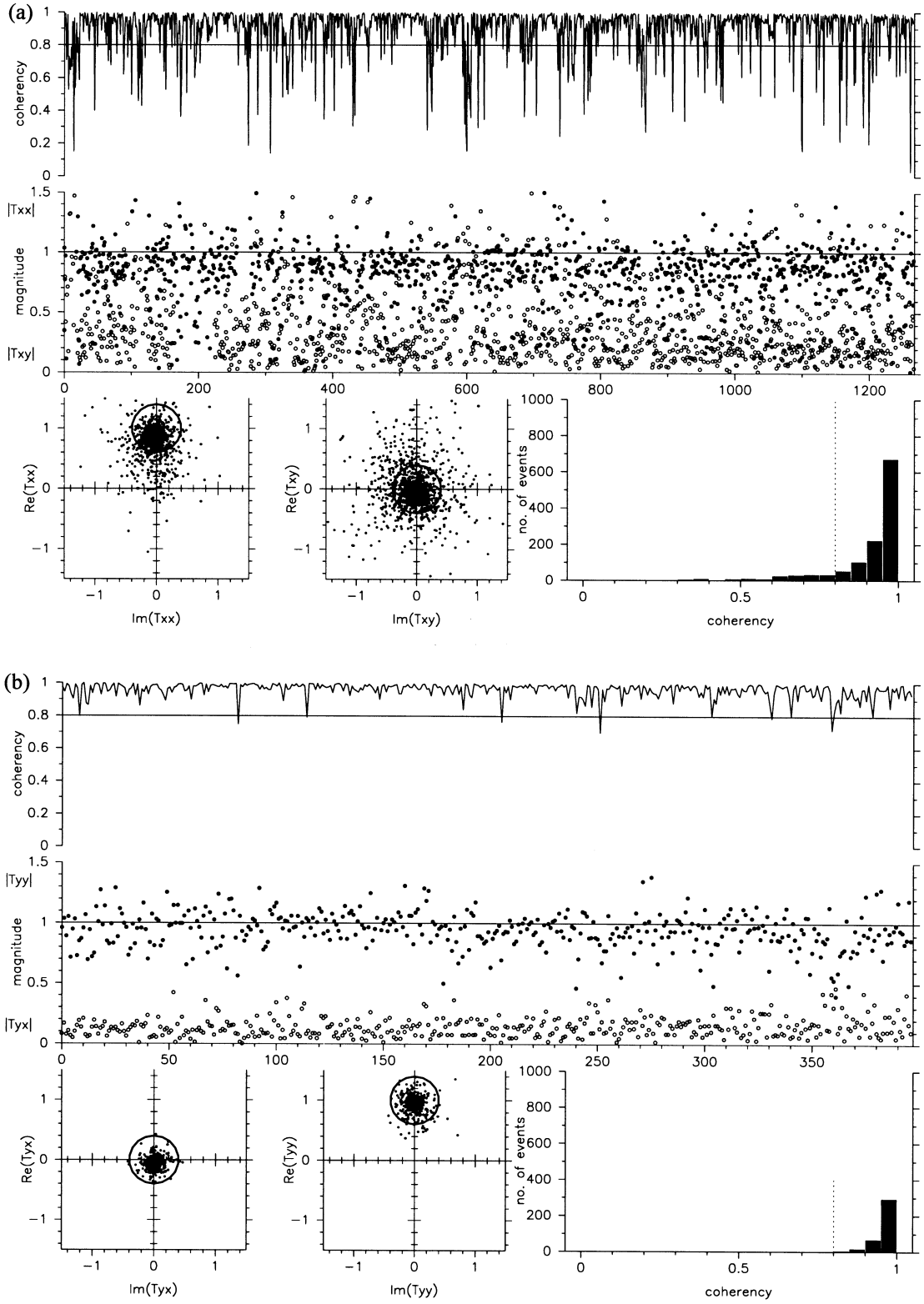

Figure 7. The effects of the source-field criterion at 16 Hz: coherencies and MRFs (a) between B_x(L008) and $B_{x,y}$(BASE); (b) between B_y(L008) and $B_{x,y}$(BASE). All estimates are derived from 1267 time-series segments (events) of 512 samples each. The top diagram shows the multiple coherency; the threshold is 0.8. Plotted just below are the magnitudes of the MRFs. The two smaller diagrams at the bottom left show the MRFs in the complex plane; the circles indicate areas of acceptance. The histogram at the bottom right gives the distribution of the coherencies. After the third decimation step in (b), more than 50 per cent of the data are rejected (see text).

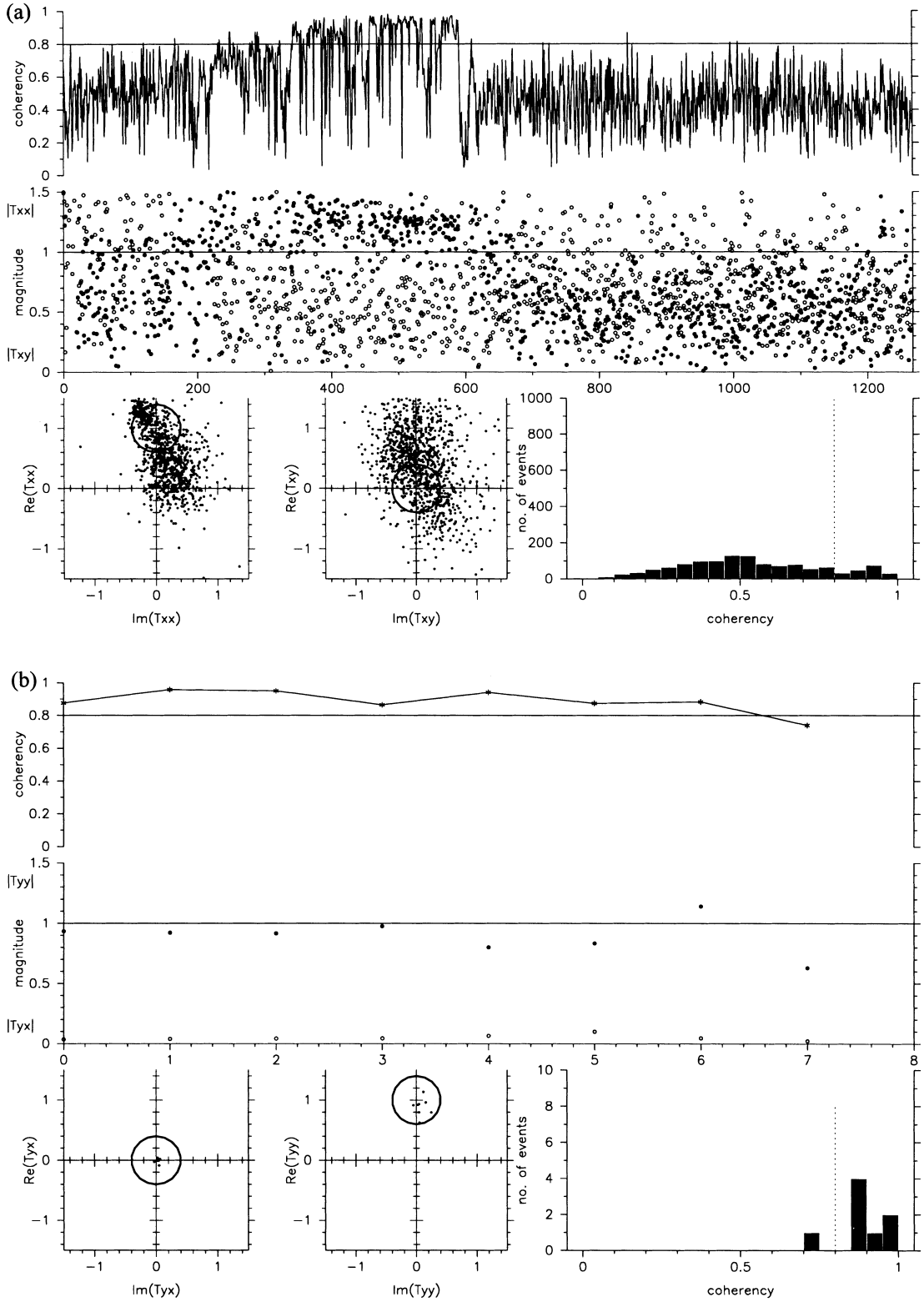

Figure 8. The effects of the source-field criterion at 45 Hz; see Fig. 7 for an explanation of the diagrams. The centre frequency of 45 Hz is close the frequency of the mains power supply (50 Hz), which is known to be generated very locally and to dominate the natural signal. More than 1000 events fail to reach the required coherency of 0.8. The distribution of the MRFs in the complex plane appears almost as random. Only eight events out of 1267 are taken over to the third decimation step in part (b) of the figure.

GJI000 18/2/98 09:10:20 3B2 version 5.20
The Charlesworth Group, Huddersfield 01484 517077

the data are reduced by the source field criterion. As expected, the amount of accepted data depends strongly on the natural signal activity. In frequency bands 0 and 1, all those frequencies that are multiples of 8 have a high volume of accepted events, very probably because they are centred around the energy maxima of the Schumann resonances. The frequency range of minimal natural signal activity, the so-called *dead band*, between 0.1 and 10 s is recognizable by the low number of accepted events. The reprocessing results of the MRFs using the cleaned data set are plotted in Figs 6(c) and (d). The curves show that the application of the source field criterion can recover a close-to-unity response over the whole frequency range at both local sites.

Generally, we find that a lot more data are rejected than accepted by the source field criterion, which means that we reduce the number of degrees of freedom. In the example in Table 2, the effect is so strong that it becomes statistically questionable to calculate variances for the highest and lowest evaluation frequencies. In practice, the method is probably most useful in audiomagnetotelluric applications for which huge data sets can be collected in short periods of time. However, the main point is that we must not feed the robust algorithm with invalid data (noise on the dependent channels). This is clearly proven in Figs 9 and 10, which show robust single site and remote reference reprocessing results using the cleaned data sets. The results of the two local sites have changed from effectively being useless to curves that can be interpreted. The error bars of the remote reference processed data in Fig. 10 are clearly larger than those of Fig. 9. The error bars are larger because the remote reference method is minimizing the covariance between the residuals estimated using both the local and remote magnetic fields. In a single site processing, the variance of the residual using local fields only is being minimized, which will usually result in smaller error bars, but not necessarily a better answer. However, the greatly improved response function results and cleaned MRFs suggest that the source field criterion can also help to reduce effectively the influence of coherent noise.

5 CONCLUSIONS

In this paper we stress the importance of high-quality horizontal magnetic field components for a meaningful estimation of geomagnetic and magnetotelluric response functions. We introduce the source-field quality criterion as a simple but efficient method to remove noise from magnetic channels in data sets of synchronously recorded sites.

Typically, all observed electromagnetic field components are contaminated to some extent with noise. The outcome of automatic data-processing schemes will therefore often be disappointing, even if robust remote reference procedures are applied. Robust (and least-squares) algorithms work generally on the basis that the input channels are free of noise, otherwise the results will be biased. The remote reference method in combination with robust processing alone cannot always improve the situation, as its successful application requires low-noise, coherent magnetic field channels from both local and remote sites. The processing of the field data from Scotland, which comprise two strongly disturbed local sites in combination with a moderately noisy remote site, results in strongly biased and scattered single site and remote reference response function estimates, which could not be interpreted.

The source-field criterion aims to find and isolate all those time segments with non-physical or strongly inhomogeneous source fields. By examining the intersite coherencies and magnetic response functions between all horizontal magnetic field components, events with poor properties are excluded from the subsequent robust stacking. The reprocessing of the remaining, strongly decimated data set results in dramatically improved vertical magnetic field response function curves for both the single site and the remote reference cases. Of course,

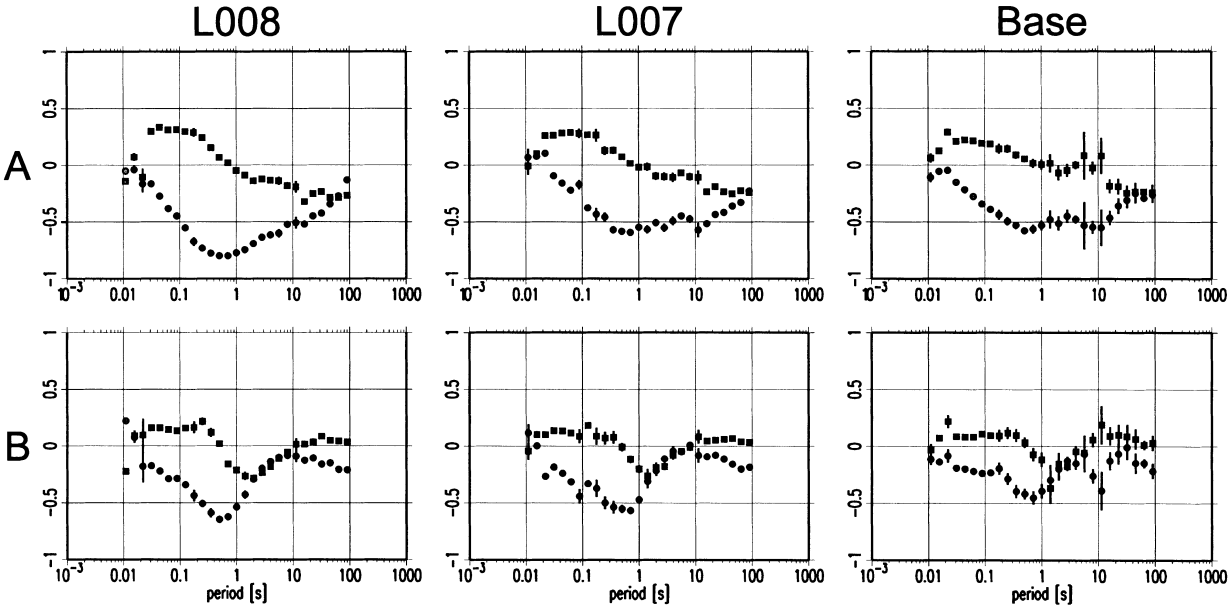

Figure 9. Robust single-site reprocessing of all sites with cleaned source fields. The results of all sites are tremendously improved over those from Fig. 3. The results of the two local sites have changed from being effectively useless, to curves that can be interpreted.

GJI000 18/2/98 09:10:30 3B2 version 5.20
The Charlesworth Group, Huddersfield 01484 517077

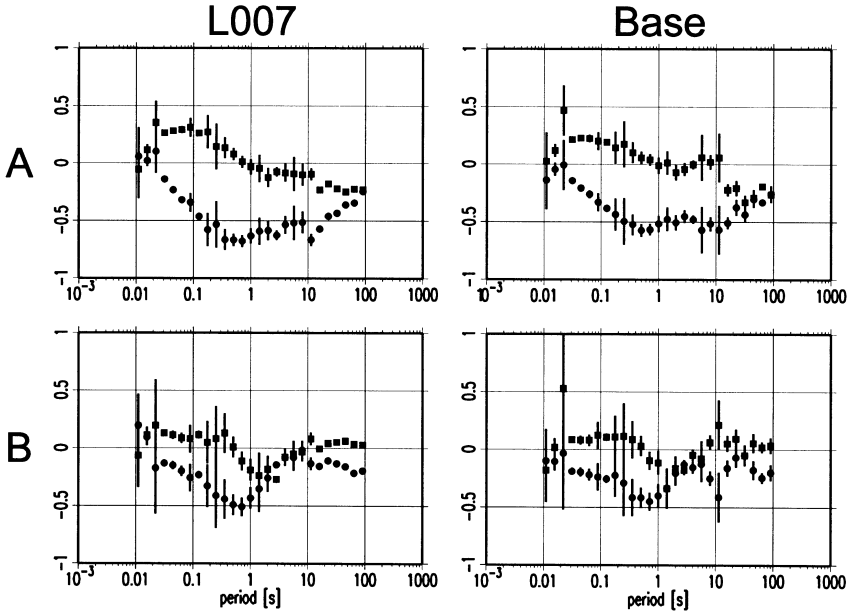

Figure 10. Robust remote reference processing of sites L007 and BASE using the cleaned data; L008 is used as the reference site. A clear improvement when compared with Fig. 4. The curves are in good agreement with the single-site reprocessing results of Fig. 9.

robust processing of the cleaned data set is still required, as the source-field criterion cannot consider outliers in the output channels.

In the past, it was often difficult to collect synchronous, multichannel recordings of high-frequency data because of hardware restrictions. Electromagnetic noise is often generated very locally, hence the noise situation can change within an area of only a few hundred metres across. On many occasions it will be possible to identify such noisy locations prior to long-term recordings with S.P.A.M. MkIII's real-time facilities. However, it is still essential to be able to record large volumes of synchronous time-series data in order to improve the results with post-processing. The multisensor capabilities are particularly interesting in applications in which data are collected on dense grids or profiles.

ACKNOWLEDGMENTS

We thank Darcy Nascimento for all the work he put into the design and construction of S.P.A.M. MkIII. OR was supported by an EEC research grant in the field of non-nuclear energies (B/JOUG 900018). We are grateful to Randy Mackie and an anonymous reviewer for their very helpful comments.

REFERENCES

Banks, R.J., Irving, A.A.K. & Livelybrooks, D.W., 1993. The simulation of magnetic variation anomalies using single-station data, *Phys. Earth. planet. Inter.,* **81,** 85–97.

Beaton, A. & Tukey, J., 1974. The fitting of power series, meaning polynomials, illustrated on band-spectroscopic data, *Technometrics,* **16,** 147–185.

Chave, A.D. & Thomson, D.J., 1989. Some comments on magnetotelluric response function estimation, *J. geophys. Res.,* **94**(B14), 14 215–14 225.

Chave, A.D., Thomson, D.J. & Ander, M.E., 1987. On the robust estimation of power spectra, coherencies, and transfer functions. *J. geophys. Res.,* **92**(B1), 633–648.

Dawes, G.J.K., 1990. Feasibility study for a transputer-based upgrade of the Short-Period Automatic Magnetotelluric (S.P.A.M.) system, *University of Edinburgh, NERC report F3/G6/S43.*

Egbert, G.D., 1997. Robust multiple-station magnetotelluric data processing, *Geophys. J. Int.,* **130,** 475–496.

Egbert, G.D. & Booker, J.R., 1986. Robust estimation of geomagnetic transfer functions, *Geophys. J. R. astr. Soc.,* **87,** 173–194.

Gamble, T.D., Goubau, W.M. & Clarke, J., 1979. Magnetotellurics with a remote reference, *Geophysics,* **44,** 53–68.

Goubau, W.M., Gamble, T.D. & Clarke, J., 1978. Magnetotelluric data analysis: removal of bias, *Geophysics,* **43,** 1157–1166.

Hampel, F.R., Ronchetti, E.M., Rousseeuw, P.J. & Stahel, W.J., 1986. *Robust Statistics*, Wiley, New York, NY.

Huber, P.J., 1981. *Robust Statistics,* Wiley, New York, NY.

Jones, A.G., Chave, A.D., Egbert, G., Auld, D. & Bahr, K., 1989. A comparison of techniques for magnetotelluric response function estimation, *J. geophys. Res.,* **94**(B10), 14 201–14 213.

Junge, A., 1990. Robust estimation of bivariate transfer functions, in *Protokoll Kolloquium Elektromagnetische Tiefenforschung,* pp. 75–86, eds Haak, V. & Homilius, H., DGG, Hornburg, Germany (in German).

Junge, A., 1992. On the effective number of degrees of freedom in magnetotelluric transfer function estimation, in *Protokoll Kolloquium Elektromagnetische Tiefenforschung,* pp. 139–158, eds Haak, V. & Rodemann, H., DGG, Borkheide, Germany (in German).

Junge, A., 1994. Induced telluric fields—new observations in North Germany and the Bramwald, *Habilitation Thesis,* Faculty of Physics, University of Göttingen, Germany (in German).

Junge, A., 1996. Characterization of and correction for cultural noise, *Surv. Geophys.,* **17,** 361–391.

Larsen, J.C., 1989. Transfer functions: smooth robust estimates by least-squares and remote reference methods, *Geophys. J. Int.,* **99,** 645–663.

Larsen, J.C., Mackie, R.L., Manzella, A., Fiordelisi, A. & Rieven, S., 1996. Robust smooth magnetotelluric transfer functions, *Geophys. J. Int.,* **124,** 801–819.

Nascimento, D., 1997. Magnetotelluric instrument development and application, *PhD thesis,* University of Edinburgh.

GJI000 18/2/98 09:10:35 3B2 version 5.20
The Charlesworth Group, Huddersfield 01484 517077

Park, J. & Chave, A.D., 1984. On the estimation of magnetotelluric response functions using the singular value decomposition, *Geophys. J. R. astr. Soc.,* **77,** 683–709.

Ritter, O., 1995. An audiomagnetotelluric investigation of the Southern Upland Fault: novel instrumentation, field procedures and 3D modelling, *PhD thesis,* University of Edinburgh.

Ritter, O. & Dawes, G., 1992. A transputer-based multi-station multi-technique geophysical data acquisition system—S.P.A.M. MkIII, in *Protokoll Kolloquium Elektromagnetische Tiefenforschung,* pp. 423–435, eds Haak, V. & Rodemann, H., DGG, Borkheide, Germany.

Szarka, L., 1988. Geophysical aspects of man-made electromagnetic noise in the earth—a review, *Surv. Geophys.,* **9,** 287–318.

Weaver, J.T., 1994. *Mathematical Methods for Geo-Electromagnetic Induction*, Research Studies Press, Taunton.

APPENDIX A: THE ROBUST ALGORITHM

A1 The χ^2 criterion

A1.1 Initial guess of response function estimates

The frequency-domain observations of the electromagnetic field components X, Y and Z are recorded in $l=1\ldots L$ time segments (=events). Z will be expressed as a linear combination of the components X and Y, plus an additional noise term δZ:

$$Z_l = a_l X_l + b_l Y_l + \delta Z_l \,. \tag{A1}$$

The response functions a_l and b_l are obtained as the solution of eq. (A1) by solving the normal equations for selected frequency bands containing at least five Fourier coefficients each. Then, we derive for the residuals S_l the following:

$$S_l^2 = \langle |\delta Z_l|^2 \rangle = \langle |Z_l - a_l X_l - b_l Y_l|^2 \rangle \,, \tag{A2}$$

where $\langle\ \rangle$ denotes the arithmetic mean over the products of Fourier coefficients of the respective frequency band.

A1.2 Initial guess of variance

$\hat{\sigma}_{\mathrm{M}}$ is the initial guess for the variance based on the median estimator:

$$\hat{\sigma}_{\mathrm{M}} = 1.483\ \mathrm{med}\,[|S_l - \mathrm{med}(S_l)|] \,. \tag{A3}$$

The median is more robust against outliers than the arithmetic mean (Hampel *et al.* 1986). We use $\hat{\sigma}_{\mathrm{M}}$ to define an upper limit c_{M}:

$$c_{\mathrm{M}} = 1.5\hat{\sigma}_{\mathrm{M}} \,, \tag{A4}$$

where the factor 1.5 in the above equation is a widely used value (Hampel *et al.* 1986) . The c_{M} values must be adjusted if the assumed amount of *bad* data is larger than $\approx$20 per cent outliers. c_{M} is used to calculate Huber weights w_l for each event l (Huber 1981):

$$w_l^{\mathrm{M}} = \begin{cases} 1 & \text{for } S_l \le c_{\mathrm{M}} \\ \dfrac{c_{\mathrm{M}}}{S_l} & \text{for } S_l > c_{\mathrm{M}} \end{cases} . \tag{A5}$$

Using the weights w_l^{M}, we sum up over all events,

$$\overline{\langle XY^* \rangle}^{\mathrm{M}} = \sum_{l=1}^{L} (w_l^{\mathrm{M}} \langle XY^* \rangle_l^0) \,, \tag{A6}$$

to calculate preliminary response functions a^{M} and b^{M} according to eq. (4).

A1.3 Robust estimation of response functions

To estimate the variance of the robust solution above, we must take into account the weights w_l. Using the Huber weights, the variance $\hat{\sigma}_{\mathrm{H}}$ becomes

$$\hat{\sigma}_{\mathrm{H}}^2 = \frac{L}{L_c^2} \sum_{l=1}^{L} (w_l^{\mathrm{M}} S_l^2) \,, \tag{A7}$$

where L_c is the number of weighted events with $w_l^{\mathrm{M}} = 1$ which fulfil the condition $S_l \le c_{\mathrm{M}}$ in eq. (A5).

To proceed, we replace c_{M} in eq. (A4) with $c_{\mathrm{H}} = 1.5\hat{\sigma}_{\mathrm{H}}$ and calculate the weights w_l^{H} in accordance with eq. (A5). Together with the Huber weights and using eq. (A6), we obtain new estimates for the response functions (a_{H} and b_{H}, respectively). The Huber function, used to compute the weights, cannot always sufficiently eliminate the effects of extreme outliers (Hampel *et al.* 1986).

A1.4 Tukey weights (reduction of extreme outliers)

To get rid of extreme outliers, the data are weighted again. This time, the weights w_l^{T} are calculated using Tukey's biweight function (Beaton & Tukey 1974). First we compute the variance $\hat{\sigma}_{\mathrm{T}}$ (Junge 1994, Appendix A.1):

$$\hat{\sigma}_{\mathrm{T}}^2 = \frac{\dfrac{1}{L} \displaystyle\sum_{l}^{L} (w_l^{\mathrm{H}} S_l)^2}{\dfrac{1}{L_{\mathrm{c}}} \displaystyle\sum_{l}^{L} \left(1 - \left(\frac{S_l}{c_{\mathrm{H}}}\right)^2\right)\left(1 - 5\left(\frac{S_l}{c_{\mathrm{H}}}\right)^2\right)} \,, \tag{A8}$$

and with the limit $c_{\mathrm{T}} = 6\hat{\sigma}_{\mathrm{T}}$ we obtain Tukey weights w_l^{T}:

$$w_l^{\mathrm{T}} = \begin{cases} \left(1 - \left(\dfrac{S_l}{c_{\mathrm{T}}}\right)^2\right)^2 & \text{for } S_l \le c_{\mathrm{T}} \\ 0 & \text{for } S_l > c_{\mathrm{T}} \end{cases} . \tag{A9}$$

If the assumption is correct that, except for a few outliers which had to be removed, the weighted δZ are normally distributed with variance σ_Z^2, then $\langle \delta Z \delta Z^* \rangle / \sigma_Z^2$ is a χ^2 distributed quantity with ν degrees of freedom. The number of degrees of freedom of a χ^2 distributed quantity can be estimated from the observations, as the ratio of the expected value to its variance:

$$\nu = \frac{2E\{\langle \delta Z \delta Z^* \rangle\}^2}{\mathrm{var}\{\langle \delta Z \delta Z^* \rangle\}} \approx \frac{2\left(\dfrac{1}{L}\displaystyle\sum_{l} \langle \delta Z \delta Z^* \rangle\right)^2}{\dfrac{1}{L-1}\displaystyle\sum_{l} (\langle \delta Z \delta Z^* \rangle_l - \overline{\langle \delta Z \delta Z^* \rangle})^2} \,. \tag{A10}$$

The noise distributions of the observations and their theoretical expectations are consistently in better agreement if the number of degrees of freedom is computed using eq. (A10) instead of being derived directly from the equivalent bandwidth of the spectral smoother (Junge 1994). The latter method usually leads to systematically overestimated values for ν and hence to underestimated error bars. The confidence limits are calculated using the weighted spectra, corrected number of degrees of freedom and the $F_{4,\nu-4}$ distribution.

GJI000 18/2/98 09:10:43 3B2 version 5.20
The Charlesworth Group, Huddersfield 01484 517077

A2 Consistency criterion

In the last section we declared single-event spectra data as *bad* if they had large errors based on single-event transfer functions. The influence of these outliers was reduced by down-weighting (removing) the whole event. The algorithm is founded on the assumption that the distributions of the derived response functions are constant in time. However, the response functions could be non-stationary owing to changing quality (inhomogeneity) of the source fields or to varying amounts of correlated noise which cannot be removed by the data-processing procedures.

The algorithm works iteratively; the superscript $j=0\ldots J$ denotes the iterations. The following abbreviations are used: $S_{xx}=\langle XX^*\rangle$, $S_{zx}=\langle ZX^*\rangle$ and $S_{zy}=\langle ZY^*\rangle$.

A2.1 Calculation of response functions

The response functions a and b and their related errors δZ_l are calculated from the $l=1\ldots L$ single-event spectra, for example using the χ^2 method of the previous section. For each iteration, we define a limit $c^{(j)}$:

$$c^{(j)}=1.5\sqrt{\mathrm{var}\{S^{(j)}_{\delta Z,l}\}}\,. \tag{A11}$$

A2.2 Calculation of weights

For the next iteration, weights less than 1 are calculated for events with errors greater than $c^{(j)}$:

$$(w_l^{(j+1)})^2=\begin{cases}1 & \text{for } S^{(j)}_{\delta Z,l}<c^{(j)}\\ \dfrac{c^{(j)}}{S^{(j)}_{\delta Z,l}} & \text{otherwise}\end{cases}\,. \tag{A12}$$

A2.3 Prediction of new spectra

In order to compute better response function values, we calculate new estimates for the cross- and auto spectra. An algorithm which works in a similar manner was developed by Egbert & Booker (1986) but predicts spectra instead of individual Fourier coefficients and is therefore faster. It can be shown to be similar to a Gauss–Newton scheme for solving non-linear systems. New estimates—or predictions—for single-event spectra are obtained by comparison with the stacked results from all events. The results for the $(j+1)$th iteration are

$$\langle|S^{(j+1)}_{zz,l}|^2\rangle_l=(w_l^{(j)})^2\langle|S^{(j)}_{zz,l}|^2\rangle_l+2w_l^{(j)}(1-w_l^{(j)})\,\mathscr{R}e\{\langle S^{(j)}_{zz,l}\hat{S}^{(j)*}_{zz,l}\rangle_l\}$$
$$+(1-w_l^{(j)})^2\langle|\hat{S}^{(j)}_{zz,l}|^2\rangle_l\,, \tag{A13a}$$

$$\langle S^{(j+1)}_{zx,l}\rangle_l=w^{(j)}\langle S^{(j)}_{zx,l}\rangle_l+(1-w_l^{(j)})\langle\hat{S}^{(j)}_{zx,l}\rangle_l\,, \tag{A13b}$$

$$\langle S^{(j+1)}_{zy,l}\rangle_l=w^{(j)}\langle S^{(j)}_{zy,l}\rangle_l+(1-w_l^{(j)})\langle\hat{S}^{(j)}_{zy,l}\rangle_l\,. \tag{A13c}$$

The previous jth iteration cross- and auto-spectra are calculated from the stacked results, using eq. (4):

$$\hat{S}^{(j)}_{zx}=a^{(j)}S^{(j)}_{xx}+b^{(j)}S^{(j)}_{xy}\,, \tag{A14a}$$

$$\hat{S}^{(j)}_{zy}=a^{(j)}S^{(j)}_{xy}+b^{(j)}S^{(j)}_{yy}\,, \tag{A14b}$$

$$\hat{S}^{(j)}_{zz}=|a^{(j)}|S^{(j)}_{xx}+|b^{(j)}|S^{(j)}_{yy}+2\,\mathscr{R}e\{a^{(j)}(a^{(j)})^*S^{(j)}_{xy}\}\,. \tag{A14c}$$

Steps 1 to 3 are repeated until the changes of $a^{(j)}$ and $b^{(j)}$ are less than a certain limit, e.g. <5 per cent. The algorithm works in a way that the smaller the weights $c^{(j)}$, the more a single-event spectrum is replaced by the value predicted from the response function (averaged over all spectra). For $w^{(j)}=1$ the observed spectra in eqs (A13a)–(A13c) are taken over to the next iteration unchanged, while for $w^{(j)}=0$ they are entirely replaced by those calculated in eqs (A14a)–(A14c).

The number of degrees of freedom is reduced to the same extent as the result of an event is replaced by its prediction:

$$v_l^{(j+1)}=v_l^{(j)}w_l^{(j)}\,. \tag{A15}$$

The consistency criterion is computationally more costly than the χ^2 procedure because it is based on an iterative algorithm. In practice, we found it often sufficient to rely solely on the χ^2 criterion.

GJI000 18/2/98 09:11:22 3B2 version 5.20
The Charlesworth Group, Huddersfield 01484 517077